

Towards Surface-Supported Supramolecular Architectures: Tailored Coordination Assembly of 1,4-Benzenedicarboxylate and Fe on Cu(100)

Magalí A. Lingenfelder,^[a] Hannes Spillmann,^[a] Alexandre Dmitriev,^[a] Sebastian Stepanow,^[a] Nian Lin,^{*,[a]} Johannes V. Barth,^[b, c] and Klaus Kern^[a, b]

Abstract: We present a comprehensive investigation of the modular assembly of surface-supported metal–organic coordination systems with specific topologies and high structural stability formed by vapor deposition of 1,4-benzenedicarboxylic acid molecules and iron atoms on a Cu(100) surface under ultra-high vacuum conditions. By making use of the two carboxylate moi-

eties available for lateral linkage to Fe atoms, we succeeded in the fabrication of distinct Fe–carboxylate coordination architectures at the surface by carefully

Keywords: coordination modes · iron · modular assembly · scanning probe microscopy · supramolecular chemistry

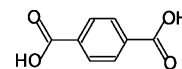
adjusting the ligand and metal concentration ratio and the temperature of the post-deposition annealing treatment. The mononuclear, 1D-polymeric and fully 2D-reticulated metallosupramolecular arrangements obtained were characterized in situ at the single-molecule level by scanning tunneling microscopy.

Introduction

In the field of supramolecular chemistry, the controlled assembly of molecules and atoms through reversible linkages (hydrogen bonding, π – π stacking, van der Waals forces, etc.) is explored, and a multitude of highly organized architectures have been synthesized from simple molecular building blocks.^[1,2] Coordination bonds, which are of intermediate strength relative to strong covalent bonding and weak non-covalent interactions such as hydrogen bonds, represent one of the most versatile and widely employed means to direct the organization of molecular building blocks into supramolecular systems with appreciable thermal stability.^[3–5] The modular assembly of coordination architectures provides a promising strategy for the preparation of novel materials. Notably, the design and synthesis of modular-assembled

metal–organic coordination networks (MOCNs) or frameworks with specific topologies and interesting properties have been achieved by using organic ligands interconnected by metallic nodes.^[3–13] The emphasis here lies in the careful choice of the polytopic organic linkers and metal atoms or metal-containing clusters used to obtain defined architectures, whose shape and properties are determined by the selected subunits. Thus, in recent years, nanoporous materials have been designed for selective molecular adsorption and storage,^[6–10] asymmetric catalysis and chiral separation,^[11] and novel magnetic phenomena^[12–15].

A simple molecular building block employed in these constructions is 1,4-benzenedicarboxylic acid (terephthalic acid, tpa).^[16] It belongs to the family of benzenepolycarboxylic



TPA

acids that provide carboxylate moieties for linkage to metal atoms, which makes this molecule suitable as a synthon in crystal engineering.^[17–21] These characteristics have been exploited for the rational design of three-dimensional nanopores,^[7–10] and very recently the capability of metal–organic frameworks containing tpa and Zn clusters for methane^[9] and hydrogen^[10] storage has been tested.

To achieve pre-designed topologies at surfaces, which is an appealing goal from both a scientific and technological

[a] M. A. Lingenfelder, Dr. H. Spillmann, Dr. A. Dmitriev, S. Stepanow, Dr. N. Lin, Prof. K. Kern
Max-Planck-Institut für Festkörperforschung
70569 Stuttgart (Germany)
Fax: (+49) 711-6891662
E-mail: n.lin@kf.mpg.de

[b] Prof. J. V. Barth, Prof. K. Kern
Institut de Physique des Nanostructures
Ecole Polytechnique Fédérale de Lausanne
1015 Lausanne (Switzerland)

[c] Prof. J. V. Barth
Advanced Materials and Process Engineering Laboratory
University of British Columbia
Vancouver, BC V6T 1Z4 (Canada)

point of view, metal-directed assembly of molecular building blocks on suitable substrates has attracted interest: 1) it provides the potential of predictability and control over the formation of low-dimensional nanostructures and 2) the substrate can act as a template directing the deposited molecules' epitaxy and the metallosupramolecular assembly. Additionally, this approach allows the use of scanning probe techniques, such as scanning tunneling microscopy (STM), for direct imaging and structural elucidation at the single-molecule level.^[22–30] Recent results demonstrate that a combination of strategies from surface science and supramolecular chemistry provides a promising base for the rational construction of surface-supported coordination architectures with specific topologies.^[31–34]

Here we describe the construction of metal–organic architectures under ultra-high vacuum conditions formed by sequential vapor deposition of terephthalic acid (tpa) and iron on an atomically clean Cu(100) surface. We present a complete structural panorama and a thorough analysis using scanning tunneling microscopy. The surface concentration of the constituents was precisely controlled and different post-deposition annealing temperatures (400 and 450 K) were employed. The role of metal–ligand interactions, which are possibly assisted by hydrogen bonding, in the stabilization of specific metallosupramolecular arrangements and their mesoscopic ordering is discussed in detail. The findings elucidate the basic principles controlling the assembly of well-defined metal–organic coordination systems from organic molecular building blocks and metal atoms on surfaces.

Results and Discussion

The molecular precursor layer: Upon deposition of tpa submonolayer doses on the Cu(100) substrate at room temperature, well-ordered two-dimensional molecular domains evolve. As shown in the large scale STM image depicted in Figure 1, close-packed tpa arrangements extend over all the

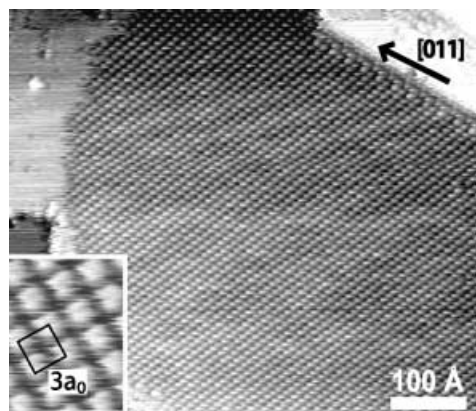


Figure 1. STM topograph of the molecular precursor layer comprising 1,4-benzenedicarboxylic acid (tpa) domains on Cu(100). The topology of the (3×3) superstructure is shown in the bottom inset; individual tpa molecules are resolved as four-lobe rhomb-shaped protrusions with a diagonal extension of 7 Å. $a_0 = 2.55$ Å is the nearest-neighbor spacing of the Cu substrate atoms.

terraces. A detailed analysis of the STM data shows that the packing of the molecules follows the Cu(100) high-symmetry directions, indicating that the substrate acts as a template directing the molecular order. The local arrangement of the molecules is characterized by a $[3 \times 3]$ unit cell (inset Figure 1). A complementary near-edge X-ray adsorption fine structure (NEXAFS) analysis revealed that the tpa molecules are adsorbed on the surface with the phenyl rings parallel to the surface plane, that is, in a flat-lying geometry.^[35] The individual tpa molecules are imaged as a rhomb-shaped protrusion with a diagonal extension of 7 Å, which agrees well with the molecular dimensions (cf. the high-resolution image in the inset in Figure 1). X-ray photoemission (XPS) experiments strongly suggest that the carboxylic groups of the tpa molecules are deprotonated in response to the catalytic activity of the substrate.^[31–34] The resulting carboxylate moieties provide reactive ligands for the formation of the coordination systems discussed below.

Synthesis of coordination architectures: To obtain arrangements in which metal centers connect to organic molecules, we deposited Fe atoms on top of the precursor layer and annealed the sample at elevated temperatures, 400–500 K. The carboxylate groups of the tpa molecules bind to the deposited Fe atoms and well-ordered structures evolve. The influence of the metal substrate on the Fe–carboxylate coordination bonds, for example, charge transfer and screening induced by the free electrons at the surface, cannot be neglected^[31] and is currently under theoretical investigation. The present findings also point to the potential role of weak hydrogen bonding in assisting the dominating metal–ligand interactions in the formation of specific metallosupramolecular arrangements and their mesoscopic ordering at surfaces. However, for a full understanding of the contributions to the stabilization of the observed architectures, in which substrate-mediated interactions or packing effects may also interfere, more detailed investigations are required.

Here we focus on establishing the parameters for the controlled formation of coordination architectures and their structural characterization. By carefully choosing the Fe concentration, distinct low-dimensional metal–organic coordination structures can be obtained that are thermally stable up to at least 500 K annealing. The structures presented in this section were obtained upon 400 K annealing for 5 minutes; the effect of treatment at higher temperatures is discussed in the next section.

Arrays of mononuclear compounds—“cloverleaf phase”: At low Fe to tpa ratios (~ 0.3 Fe atoms per tpa molecule), arrays of mononuclear metal–organic complexes evolve (Figure 2a). The high-resolution image in Figure 2b reveals that the individual complexes resemble cloverleaves with four tpa molecules surrounding a central Fe atom. Similar cloverleaf-shaped metal–organic arrangements have already been encountered in related systems.^[31,32] STM imaging cannot provide direct information about intermolecular interactions and bonding, but the accurate topology obtained from high-resolution STM data enables us to suggest structural models to be verified or refined by other experimental

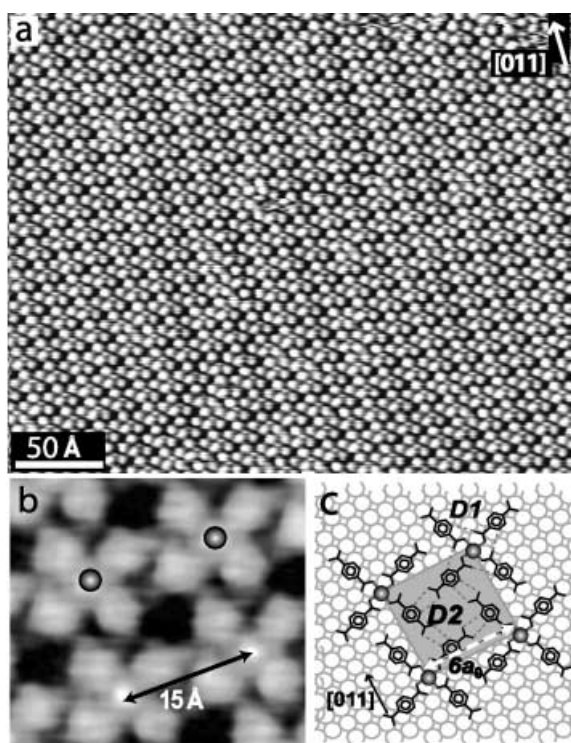


Figure 2. a) STM image of the “cloverleaf phase”. b) High-resolution STM image with Fe atoms marked. c) Geometrical model: each Fe atom (gray spheres) coordinates four carboxylate ligands unidentately in a square-planar configuration. Potential C–H...O hydrogen bonds are indicated (O...H–C distance $D1 = D2 = 3.5 \text{ \AA}$). The $15 \times 15 \text{ \AA}^2$ superstructure unit cell is shown as a gray square.

techniques. Based on a careful analysis of the data the model in Figure 2c is proposed for the mononuclear complex, $[\text{Fe}(\text{tpa})_4]$. It consists of a central Fe atom (gray sphere) coordinated to four tpa molecules in a square-planar structure by unidentate Fe–carboxylate bonds with an Fe–O distance of approximately 2 \AA . The distance between the carboxylate oxygen and phenyl ring carbon (O...H–C, marked by dashed lines $D1$ in Figure 2c) is $\sim 3.5 \text{ \AA}$, and thus may be associated with an interaction that is potentially hydrogen bonding.^[36] There is experimental evidence that (weak) intermolecular hydrogen bonds evolve when appropriate functional groups of adsorbed molecules are at reasonable distances.^[37–40] With the systems investigated so far the bonding distances are typically increased relative to related coupling schemes in organic bulk materials.^[30] In view of the fact that the carboxylate group is a strong hydrogen-bond acceptor, it is tentatively suggested that the $[\text{Fe}(\text{tpa})_4]$ arrangement may be further stabilized by intracomplex C–H...O hydrogen bonding.

The complexes are organized in a $[6 \times 6]$ unit cell with respect to the substrate as shown by the gray square in the model (Figure 2b) and form a well-ordered array covering all the terraces of the substrate. This perfect long-range organization suggests intercomplex interactions. Since the distance between the carbon atom in the *ortho*-position of the ring and oxygen atom of the carboxylate group (see dashed line $D2$ in Figure 2c) is 3.5 \AA , the interaction between the

hydrogen in the *ortho*-position of the ring and the carboxylate group again can be considered as potentially hydrogen bonding and a coupling in the dihapto mode between the strong COO^- acceptor and C–H groups of the phenyl ring is tentatively suggested.^[36] For modeling purposes we assume that the Fe atoms reside at the energetically preferred hollow site of the substrate. The individual Fe atoms are separated from each other by 15 \AA in both directions, forming a perfect 2D array at the surface.

A close inspection of the high-resolution image and model reveals that a given tpa molecule in the $[\text{Fe}(\text{tpa})_4]$ complex coordinates to the central Fe atom through the “left-hand” oxygen atom of the carboxylate moiety, which leads to a $P4$ symmetry for the cloverleaf structure. $[\text{Fe}(\text{tpa})_4]$ complexes with “right-hand” oxygen coordination were similarly encountered at the surface. The “left-” and “right-hand” coordination modes fold the cloverleaf complexes in opposite directions (clockwise and anticlockwise, respectively) and consequently they are nonsuperimposable upon in-plane rotation or translation: one type represents the mirror image of the other with respect to the Cu $[011]$ azimuth, that is, they are two enantiomeric species.^[32] Moreover, each single array of packed complexes only consists of cloverleaves of one handedness (like the one presented in Figure 2); this which signals chiroselective intercomplex interactions, presumably mediated by the suspected intercomplex hydrogen bonding.

MOCN-I—“ladder phase”: At higher Fe concentrations (~ 0.8 atoms per tpa molecule) an extended network structure evolves, labeled the MOCN-I phase (Figure 3). This phase is characterized by double rows of tpa molecules running along the $[011]$ or $[\bar{0}\bar{1}\bar{1}]$ direction of the substrate, as indicated (DR) in the inset of Figure 3. The spacing between the double rows again indicates potential intrarow C–H...O hydrogen bonds between the H atom in the *ortho* position of the phenyl ring and the carboxylate moiety, as depicted in the corresponding model (dashed lines in Figure 3b, O...H–C distance $D1 = 3.0 \text{ \AA}$).

Adjacent double rows are linked by tpa molecules perpendicular to the double-row directions, designated spacer tpa, by Fe–carboxylate formation. Each Fe atom (highlighted by gray spheres in the inset of Figure 3a) is coordinated to three tpa molecules: two double-row tpa and one spacer tpa. The double-row tpa molecules are linked by means of unidentate bonds to the Fe, and the spacer tpa by a chelating bidentate bond, forming a distorted square-planar geometry. Similar coordination motifs have been reported in layer structures of 3D crystals.^[18] Two different types of the MOCN-I phase can be distinguished depending on how the double rows are linked by the spacer tpa molecules. The first kind is marked with a rectangle in the STM image and in the geometric model (Figures 3a and 3b, respectively), whereby two neighboring double rows are coupled by a column of single tpa spacer molecules. Each end of the spacer tpa is coordinated to an Fe atom at the neighboring double rows. The gap between the neighboring double rows is 10 \AA ($4a_0$), and the lateral distance between the equally aligned spacer tpa molecules is also 10 \AA ($4a_0$). Owing to

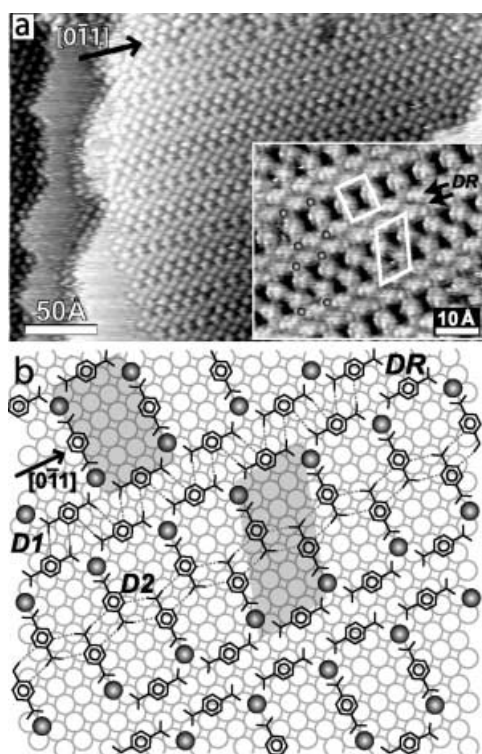


Figure 3. a) STM image of the 1D MOCN-I “ladder phase”. Fe atom positions are marked by gray spheres and a double row by DR. b) Geometrical model of the MOCN-I phase: dashed lines D1 (D2) indicate potential interrow (intrarow) C–H...O hydrogen bonds (in both cases the O...H–C distance is 3.0 Å).

the fact that Fe–carboxylate coordination only propagates along the double-row directions but not perpendicularly, a 1D ladder configuration forms, representing a 1D polymeric coordination system. The dark areas in the STM topograph, framed by the tpa networks, correspond to cavities in which the Cu substrate is exposed. These cavities have a distinct shape, size ($\sim 10 \times 3$ Å), and regular 1D order with a spacing of 10 Å.

The second type of MOCN-I phase is marked with a rhomb in the STM image and in the geometric model (Figure 3a and 3b), whereby neighboring double rows are linked by two columns of spacer tpa molecules. The Fe coordination is the same as in the former case, but only one carboxylate group of the spacer tpa is coordinated to the iron atoms now. The spacer tpa molecules that are coordinated to the upper and lower double rows are staggered; this arrangement suggests potential C–H...O hydrogen bonds between the H atoms in the *ortho* positions of the phenyl ring and the carboxylate groups, as depicted in the model (dashed line in Figure 3b, O...H–C distance $D2 = 3.0$ Å). This configuration accounts for a wider gap, 15 Å ($6a_0$), between the double rows and displays well-defined cavities arranged in a zigzag pattern with a size smaller than the previous case, $\sim 5 \times 3$ Å.

Stoichiometrically the first type of phase has a higher Fe to tpa ratio (ideally $\frac{2}{3}$ for type 1 and $\frac{4}{9}$ for type 2), which is in agreement with our observation that further increasing the Fe concentration raises the fraction of the type 1

MOCN-I phase. However, we could not obtain pure phases of either type.

MOCN-II—“single-row phase”: Upon increasing the Fe to tpa ratio to about 1.2 the MOCN-II phase develops (Figure 4a). STM data reveal the formation of domains with a

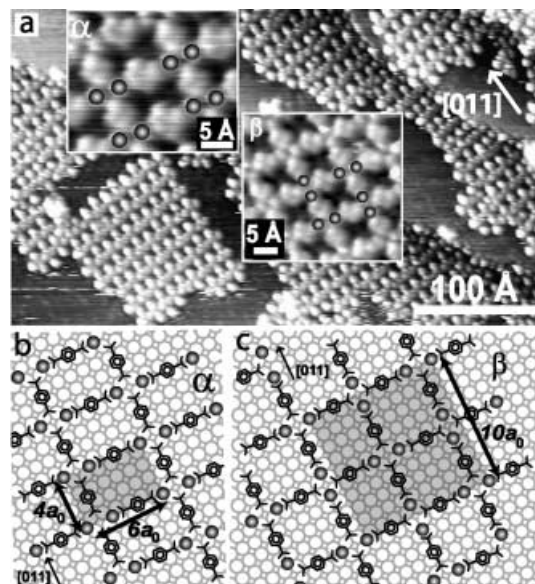


Figure 4. a) STM image of the 2D reticulated MOCN-II “single-row phase”. High-resolution STM images reveal the geometrical arrangements in the α (upper inset) and β (bottom inset) phases, which differ in the orientation of the neighboring iron pairs. b) and c) Geometrical models depicting atomic and molecular positioning in the two isomeric structures and the corresponding unit cells.

typical size of 15×15 nm. The fully 2D reticulated structures of the MOCN-II fall into two classes, labeled α and β , which always co-exist at the surface. They are identified as isomeric structures, since they evolve simultaneously and exhibit the same building blocks and stoichiometry ($\text{Fe}/\text{tpa} = 1$).^[33] In the α phase (upper inset of Figure 4a), the reticular structure and the coordination geometry are very similar to those of the first type MOCN-I phase; only the double tpa rows are replaced by single tpa rows here, that is, single rows are linked by a column of single spacer tpa molecules. As a consequence at every network junction two Fe atoms are present, forming an iron pair with an Fe–Fe spacing of 5 Å ($2a_0$). These iron pairs are linked by tpa molecules through Fe–O coordination and organized in a $6a_0 \times 4a_0$ repeat unit (model in Figure 4b). Well-defined cavities, equivalent to those found in the first type MOCN-I phase, are also present here.

In the β phase (lower inset in Figure 4a), the orientations of the iron pairs alternate, that is, each iron pair is rotated by 90° with respect to its nearest neighbors. To adopt such an arrangement a given tpa molecule must have one bidentate and two unidentate bonds at its respective ends. The network topology displays a square symmetry, and the size of the repeating unit cell in this case is $10a_0 \times 10a_0$ (model in

Figure 4c). The cavities are square in shape with concave edges, and have a size of $\sim 7 \times 7 \text{ \AA}$.

Influence of the post-deposition annealing temperature and the molecular coverage conditions:

In order to obtain a better understanding of the influence of the temperature on the synthesis of the metal–organic networks, we studied the effect of post-deposition annealing. After the deposition of the tpa molecules and Fe on the substrate at room temperature, we annealed the sample at 450 K instead of 400 K. Under these new conditions all the coordination architectures produced by 400 K annealing could be obtained. However, the Fe/tpa ratios necessary for the construction of a given structure always exceeded those required for 400 K annealing. This is presumably related to an increased tendency for Fe–Cu-surface intermixing at higher substrate temperatures; hence less Fe is available for metal–organic coordination networks.^[41–43] Table 1 summarizes the Fe/tpa surface concentration ratios required to obtain the various structures under the two different annealing conditions.

Table 1. Fe/tpa surface concentration ratios required for the fabrication of the metal–organic coordination structures at the annealing temperatures employed.

Annealing temperature [K]	Fe:tpa ratio			
	cloverleaf	MOCN-I	MOCN-II	MOCN-III
400	0.3	0.8	1.2	–
450	0.4	1.0	1.5	0.9

Scheme 1 gives an overview of the compounds described in this paper. In addition, with 450–500 K annealing we observed the development of a new phase which does not form upon 400 K annealing.

MOCN-III—“interlocked phase”: For an Fe concentration of about 0.9 atoms per tpa molecule deposited on the molecular precursor layer that is close to saturation ($\sim 80\%$ monolayer) the MOCN-III phase develops. As shown in Figure 5, this phase covers all of the terraces and can be viewed as an interruption of single rows along the direction normal to the iron pairs, as indicated by the broken line in Figure 5a. The broken parts are shifted laterally by half of the single-row separation. The network structure extends continuously in the direction perpendicular to the broken rows. As shown in Figure 5a the interruption occurs typically at every third (solid-line rectangle in Figure 5a) or every fourth unit (dashed-line rectangle in Figure 5a), but structures with a width of up to six units also exist. The broken rows are interlocked with each other. The spacing between the carboxylate group oxygen and the *ortho* hydrogen atom on the phenyl ring ($\text{O}\cdots\text{H}-\text{C}$ distance $D=3.1 \text{ \AA}$, dashed lines in Figure 5b) indicates potential hydrogen bonding; the corresponding dihapto hydrogen-bond motif is marked in Figure 5b.

Figure 6a shows an extreme case of the interlocked phase obtained upon depositing iron on top of a completed tpa monolayer. It consists of interlocked single rows of just one unit. Once again, the model suggests potential hydrogen

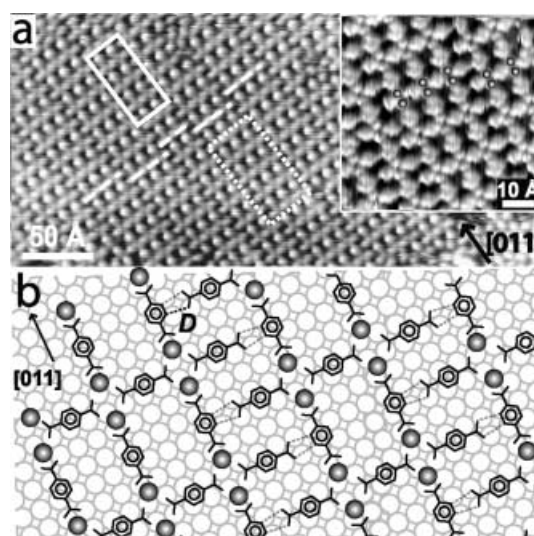


Figure 5. a) STM image of the MOCN-III “interlocked phase”. The solid and dashed rectangles indicate two and three complex units (inset: high resolution STM image). b) Geometrical model of MOCN-III (Fe: gray spheres) with potential intermolecular C–H \cdots O hydrogen bonds indicated ($\text{O}\cdots\text{H}-\text{C}$ distance $D=3.1 \text{ \AA}$).

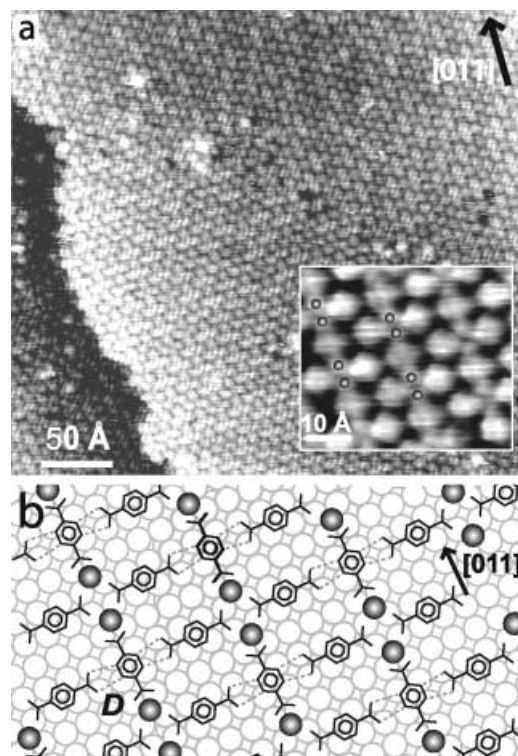
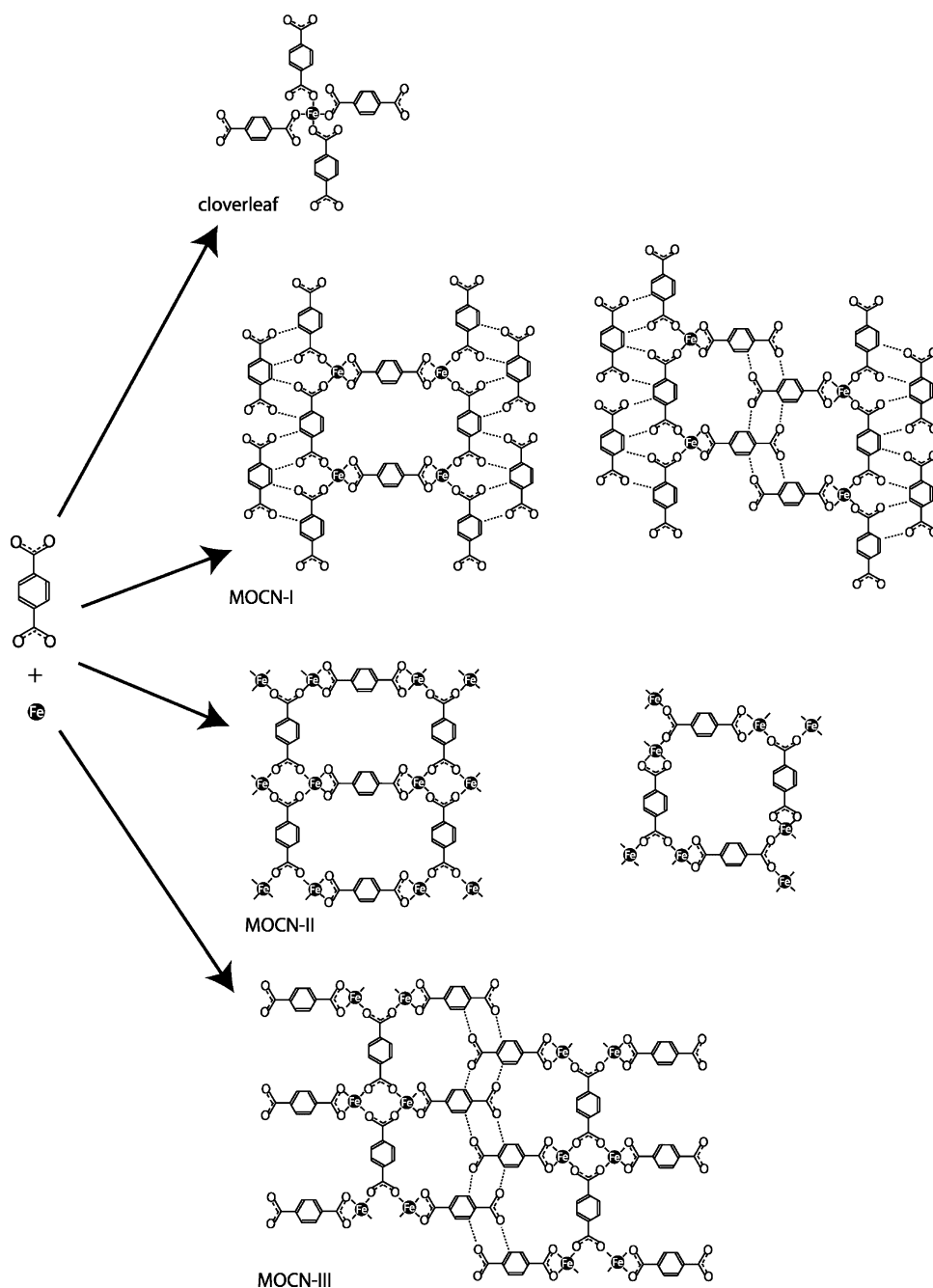


Figure 6. a) STM image of the single-unit “interlocked phase”; the inset shows a high resolution STM image (Fe: gray spheres). b) Geometrical model with potential C–H \cdots O hydrogen bonds indicated ($\text{O}\cdots\text{H}-\text{C}$ distance $D=3.1 \text{ \AA}$).

bonds between the oxygen atom of the carboxylate group and the *ortho* H of the neighboring phenyl ring in dihapto mode ($\text{O}\cdots\text{H}-\text{C}$ distance $D=3.1 \text{ \AA}$; dashed lines in Figure 6b). This arrangement accommodates the highest density of tpa molecules and iron pairs that can be obtained on the surface.



Scheme 1. Overview of the compounds synthesized at different Fe:tpa ratios.

Conclusion

In conclusion, while crystal engineers concentrate their efforts on designing metal-organic architectures by choosing appropriate metal centers, ligands and crystallization conditions, we have explored the deposition parameters (temperature, surface concentration, etc.) required to achieve the modular assembly of distinct surface-supported coordination architectures. Strategies to synthesize different metal-organic structures with other benzenepolycarboxylic acids molecules have also been developed.^[32–34] Fe-carboxylate coordination at metal surfaces is thus known for several systems

and can be used to fabricate a variety of distinct metal-organic architectures. This approach presents a step towards a new synthetic route to novel low-dimensional metal-organic materials.

In general, all the structures fabricated in this work are composed of regular arrangements of iron centers or iron pairs. Taking into account the magnetic character of Fe, cooperative magnetic coupling in coordination systems mediated by the spacer molecules or the Cu substrate is feasible, making them potential low-dimensional molecule-based magnetic systems. The well-defined cavity envelope in the MOCNs allows the use of these nanopores in selective adsorption processes. Notably the reversible adsorption of C_{60} guest molecules in such cavities has been successfully demonstrated recently.^[44] Further experiments addressing inclusion phenomena with alkali metals are in progress. Moreover, interesting properties for heterogeneous catalysis can be envisioned. The combination of an organic recognition subunit connected to a reactive metal site offers prospects for catalysts with shape, regio-, and stereoselectivity. For example, the iron pairs resemble active sites in carboxylate-bridged non-heme diiron enzymes.^[45] Finally we envision the use of metal-organic grids as multifunctional nanotemplates to steer the growth of three-dimensional architectures.

Experimental Section

The experiments were performed in an ultra-high vacuum system equipped with sample preparation tools, evaporators for organic molecule and metal deposition and a home-built STM. The Cu(100) surface was cleaned by repeated cycles of Ar^+ sputtering at room temperature and subsequent annealing to 800 K. This cleaning procedure resulted in atomically clean terraces of up to 100 nm width separated by monatomic steps. Terephthalic acid (tpa) (99%, Fluka) was deposited under UHV conditions (background pressure $\sim 3 \times 10^{-10}$ mbar) by organic molecular beam epitaxy (OMBE) from a Knudsen cell type evaporator, maintained at 440 K during deposition. The molecular evaporation was monitored by

using a quadrupole mass spectrometry (QMS) analysis system, which also showed that evaporation produces a beam of intact molecular species. Fe atoms were evaporated using an e-beam heating evaporator. To limit the surface intermixing that can occur in the pure Fe/Cu(100) system,^[41a,b] Fe was always deposited on top of the organic layer. The actual surface concentration ratio necessary to obtain a given structure generally exceeded the ideal stoichiometric ratio extracted from the models, which is attributed to the loss of Fe atoms in other surface processes, such as decoration of the substrate steps, Fe-island formation and additional Fe–Cu intermixing processes.^[41–43] Table 2 summarizes the estimated Fe loss for the

Table 2. Estimated Fe loss for the structures generated at different coverages and annealing temperatures.

Annealing temperature [K]	cloverleaf	Estimated Fe loss [%]		
		MOCN-I	MOCN-II	MOCN-III
400	16	17	20	–
450	38	34	33	27

structures generated at different coverages and annealing temperatures. Both organic and metal deposition were performed with the substrate at room temperature, with subsequent annealing to 400 or 450 K to increase the mobility of the molecules and to overcome the activation barrier for the formation of metal–organic arrangements. STM experiments employing the constant current mode were subsequently performed in situ after cooling to room temperature.

- [1] J. M. Lehn, *Supramolecular Chemistry: Concepts and Perspectives*, VCH, New York, **1995**.
- [2] T. D. Tullius in *Comprehensive Supramolecular Chemistry*, Vol. 5 (Eds.: J. L. Atwood, J. E. D. Davies, D. D. MacNicol, F. Vögtle, K. S. Suslick, J.-M. Lehn), Pergamon, Oxford, **1996**.
- [3] S. R. Seidel, P. J. Stang, *Acc. Chem. Res.* **2002**, *35*, 972–983.
- [4] B. J. Holliday, C. A. Mirkin, *Angew. Chem.* **2001**, *113*, 2076–2098; *Angew. Chem. Int. Ed.* **2001**, *40*, 2022–2043.
- [5] J.-P. Sauvage, *Transition Metals in Supramolecular Chemistry*, Wiley-VCH, Weinheim, **1999**.
- [6] M. E. Kosal, J. Chou, S. R. Wilson, K. S. Suslick, *Nat. Mater.* **2002**, *1*, 118–121.
- [7] M. Eddaoudi, H. Li, O. M. Yaghi, *J. Am. Chem. Soc.* **2000**, *122*, 1391–1397.
- [8] H. Li, M. Eddaoudi, T. L. Groy, O. M. Yaghi, *J. Am. Chem. Soc.* **1998**, *120*, 8571–8672.
- [9] M. Eddaoudi, J. Kim, N. Rosi, D. Vodak, J. Wachter, M. O’Keeffe, O. M. Yaghi, *Science* **2002**, *295*, 469–472.
- [10] N. Rosi, J. Eckert, M. Eddaoudi, T. Vodak, J. Kim, M. O’Keeffe, O. M. Yaghi, *Science* **2003**, *300*, 1127–1129.
- [11] J. Seo, D. Whang, H. Lee, S. Jun, J. Oh, Y. Jeon, K. Kim, *Nature* **2000**, *404*, 982–986.
- [12] B. Moulton, J. J. Lu, R. Hajndl, S. Hariharan, M. J. Zaworotko, *Angew. Chem.* **2002**, *115*, 2945–2948; *Angew. Chem. Int. Ed.* **2002**, *41*, 2821–2824.
- [13] H. Srikanth, R. Hajndl, B. Moulton, M. J. Zaworotko, *J. Appl. Phys.* **2003**, *93*, 7089–7091.
- [14] D. Maspoch, D. Ruiz-Molina, K. Wurst, N. Domingo, M. Cavallini, F. Biscarini, J. Tejada, C. Rovira, J. Veciana, *Nat. Mater.* **2003**, *2*, 190–195.
- [15] S. Chui, S. Lo, J. Charmant, A. Orpen, I. Williams, *Science* **1999**, *283*, 1148–1150.
- [16] M. Sledz, J. Janczak, R. Kubiak, *J. Mol. Struct.* **2001**, *595*, 77–82.
- [17] M. Eddaoudi, D. Moler, H. Li, T. M. Reineke, M. O’Keeffe, O. M. Yaghi, *Acc. Chem. Res.* **2001**, *34*, 319–330.
- [18] L. Pan, N. Ching, X. Y. Huang, J. Li, *Inorg. Chem.* **2000**, *39*, 5333–5340.
- [19] S. Bourne, A. Mondal, M. Zaworotko, *Cryst. Eng.* **2001**, *4*, 25–36.
- [20] Z. Fu, X. Wu, J. Dai, S. Hu, W. Du, H. Zhang, R. Sun, *Eur. J. Inorg. Chem.* **2002**, 2730–2735.
- [21] Y. Cui, O. R. Evans, H. L. Ngo, P. S. White, W. Lin, *Angew. Chem.* **2002**, *114*, 1207–1210; *Angew. Chem. Int. Ed.* **2002**, *41*, 7, 1159–1162.
- [22] A. Hatzor, T. Moav, H. Cohen, S. Matlis, J. Libman, A. Vaskevich, A. Shanzler, I. Rubinstein, *J. Am. Chem. Soc.* **1998**, *120*, 13469–13477.
- [23] A. Semenov, J. P. Spatz, M. Möller, J. M. Lehn, B. Sell, D. Schubert, C. H. Weidl, U. S. Schubert, *Angew. Chem.* **1999**, *111*, 2701–2705; *Angew. Chem. Int. Ed.* **1999**, *38* 2547–2550.
- [24] I. Weissbuch, P. N. W. Baxter, I. Kuzmenko, H. Cohen, S. Cohen, K. Kjaer, P. B. Howes, J. Als-Nielsen, J. M. Lehn, L. Leiserowitz, M. Lahav, *Chem. Eur. J.* **2000**, *6*, 725–734.
- [25] S. A. Levi, P. Guatteri, F. C. J. M. v. Veggel, G. J. Vansco, E. Dalcanale, D. N. Reinhoudt, *Angew. Chem.* **2001**, *113*, 1945–1948; *Angew. Chem. Int. Ed.* **2001**, *40*, 1892–1896.
- [26] U. Ziener, J. M. Lehn, A. Mourran, M. Möller, *Chem. Eur. J.* **2002**, *8*, 951–957.
- [27] D. G. Kurth, N. Severin, J. P. Rabe, *Angew. Chem.* **2002**, *114*, 3833–3835; *Angew. Chem. Int. Ed.* **2002**, *41*, 3681–3683.
- [28] D. Wouters, S. Höppener, R. Lunkwitz, L. Chi, H. Fuchs, U. S. Schubert, *Adv. Funct. Mater.* **2003**, *13*, 277–280.
- [29] S. Hoepfner, L. F. Chi, H. Fuchs, *Nano Lett.* **2002**, *2*, 459–463.
- [30] S. De Feyter, F. C. De Schryver, *Chem. Soc. Rev.* **2003**, *32*, 139–150.
- [31] N. Lin, A. Dmitriev, J. Weckesser, J. V. Barth, K. Kern, *Angew. Chem.* **2002**, *114*, 4973–4977; *Angew. Chem. Int. Ed.* **2002**, *41*, 4779–4783.
- [32] P. Messina, A. Dmitriev, N. Lin, H. Spillmann, M. Abel, J. V. Barth, K. Kern, *J. Am. Chem. Soc.* **2002**, *124*, 14000–14001.
- [33] A. Dmitriev, H. Spillmann, N. Lin, J. V. Barth, K. Kern, *Angew. Chem.* **2003**, *115*, 2774–2777; *Angew. Chem. Int. Ed.* **2003**, *42*, 2670–2673.
- [34] H. Spillmann, A. Dmitriev, N. Lin, P. Messina, J. V. Barth, K. Kern, *J. Am. Chem. Soc.* **2003**, *125*, 10725–10728.
- [35] T. Strunskus, C. Wöll, private communication.
- [36] T. Steiner, *Angew. Chem.* **2002**, *114*, 50–80; *Angew. Chem. Int. Ed.* **2002**, *41*, 48–76; G. R. Desiraju, T. Steiner, *The Weak Hydrogen Bond: In Structural Chemistry and Biology* (International Union of Crystallography Monographs on Crystallography, No 9), Oxford University Press, Oxford, **2001**.
- [37] J. V. Barth, J. Weckesser, N. Lin, A. Dmitriev, K. Kern, *Appl. Phys. A* **2003**, *76*, 645–652.
- [38] M. Böhringer, K. Morgenstern, W.-D. Schneider, R. Berndt, F. Mauri, A. De Vita, R. Car, *Phys. Rev. Lett.* **1999**, *83*, 324–327.
- [39] J. V. Barth, J. Weckesser, G. Trimarchi, M. Vladimirova, A. De Vita, C. Cai, H. Brune, P. Günter, K. Kern, *J. Am. Chem. Soc.* **2002**, *124*, 7991–8000.
- [40] T. Yokoyama, S. Yokoyama, T. Kamikado, Y. Okuno, S. Mashiko, *Nature* **2001**, *413*, 619–621.
- [41] D. D. Chambliss, K. E. Johnson, *Phys. Rev. B* **1994**, *50*, 5012–5015.
- [42] J. V. Barth, D. E. Fowler, *Phys. Rev. B* **1995**, *52*, 11432–11440.
- [43] D. Spisak, J. Hafner, *Phys. Rev. B* **2001**, *64*, 205422.
- [44] S. Stepanow, M. Lingenfelder, A. Dmitriev, H. Spillmann, E. Delvigne, N. Lin, X. Deng, C. Cai, J. V. Barth, K. Kern, *Nat. Mater.* **2004**, in press.
- [45] D. Lee, S. J. Lippard, *Inorg. Chem.* **2002**, *41*, 2704–2719.

Received: October 1, 2003 [F5589]